Biochemistry and Biophysics Reports 27 (2021) 101027

Contents lists available at ScienceDirect

Biochemistry and Biophysics Reports

journal homepage: www.elsevier.com/locate/bbrep

Changes in cytoarchitecture and mobility in B16F1 melanoma cells induced by 5-Br-2'-dU coincide with Rock2, miRNAs 138-5p and 455-3p reciprocal expressions

Esther Natalia Muñoz [a,b,*], Hernán Mauricio Rivera [a], Luis Alberto Gómez [a,b,**]

[a] Molecular Physiology Group, Scientific and Technological Research, Public Health Research, Instituto Nacional de Salud de Colombia, Bogotá, D.C., Colombia
[b] Department of Physiological Sciences, Faculty of Medicine, Universidad Nacional de Colombia, Bogotá, D.C., Colombia

ARTICLE INFO

Keywords:
Melanoma
miRNAs
5-Bromo-2'-deoxyuridine
Invasion
Migration

ABSTRACT

ROCK2 is a protein involved in the restructuring of the cytoskeleton in cell adhesion and contractibility processes. miR-138-5p and miR-455-3p regulate Rock2 expression, cell proliferation, migration, and invasion in different experimental cell models. However, their participation in the cytoarchitecture and mobility of B16F1 melanoma cells exposed to 5-Br-2'-dU is partially known. This work aimed to analyze ROCK2 and miRs 138-5p and 455-3p expression associated with morphological and mobility changes of B16F1 mouse melanoma cells exposed to the thymidine analog 5-Bromo-2'-deoxyuridine (5-Br-2'-dU). We observed an increase (2.2X $n = 3$, $p < 0.05$) in the cell area, coinciding with an increase in cell diameter (1.27X $n = 3$, $p < 0.05$), as well as greater cell granularity, capacity for circularization, adhesion, which was associated with more significant polymerization of F-actin, collapsed in the intermediate filaments of vimentin (VIM), and coinciding with a decrease in migration (87%). Changes coincided with a decrease in Rock2 mRNA expression (2.88X $n = 3$, $p < 0.05$), increased vimentin and a reciprocal decrease in miR-138-5p (1.8X), and an increase in miR-455-3p (2.39X). The Rock2 kinase inhibitor Y27632 partially rescued these changes. These results suggest ROCK2 and VIM regulate the morphological and mobility changes of B16 melanoma cells after exposure to 5-Br-2'-dU, and its expression may be reciprocally regulated, at least in part, by miR-138-5p and miR-455-3p.

1. Introduction

Cutaneous melanoma is a highly invasive and metastatic cancer with a low survival rate in advanced stages [1,2]. In *in vitro* models, melanoma cells can restructure their cytoskeleton, altering their adhesion and contractibility, increasing their migration and invasion capacity. *In vitro* and *in vivo*, the inhibition of the activity of the Rho-associated protein kinase 2 (ROCK2) decreases the volume of the tumor mass in mice and the migration and metastasis in melanoma cells [3,4]. Furthermore, ROCK2 regulates cytoarchitecture through the collapse of intermediate filaments Vimentin phosphorylation (VIM) [5] and the formation of actin stress fibers by phosphorylation of the myosin light chain 2 (MLC2) and the inhibition of the phosphatase activity of the myosin light chain kinase (MLCK), which inhibits MLC2 [6,7]. However, in cells induced to senescence, there is not enough knowledge about ROCK2 involvement and regulation.

Senescent cells change various physiological aspects, including reorganizing the cytoskeleton and differential kinases expression [8,9]. There is a decrease in ROCK1 expression [9], while knockout of both ROCK1 and ROCK2 is associated with cell cycle arrest and senescence, possibly due to decreased expression CyclinA, CKS1, and CDK1 [10].

The thymidine analog, 5-Bromo-2'-deoxyuridine (5-Br-2'-dU), incorporates into the DNA, generates instability, and has been widely used in different types of cancer [11,12]. Although its mechanism of action is unknown, its exposure in B16 mouse melanoma cells induces a senescent phenotype together with changes in their extracellular matrix glycoproteins, cell attachment, adhesion-related glycoproteins to tumor cell-cell interaction and actin expression, as well as a reduction in

* Corresponding author. Molecular Physiology Group, Scientific and Technological Research, Public Health Research, Instituto Nacional de Salud de Colombia, Bogotá, D.C., Colombia.
** Corresponding author. Molecular Physiology Group, Scientific and Technological Research, Public Health Research, Instituto Nacional de Salud de Colombia, Bogotá, D.C., Colombia.
E-mail addresses: enmunozro@unal.edu.co (E.N. Muñoz), lgomez@ins.gov.co (L.A. Gómez).

https://doi.org/10.1016/j.bbrep.2021.101027
Received 14 January 2021; Received in revised form 12 May 2021; Accepted 14 May 2021

proliferation, pigmentation, and differential expression of mRNAs and microRNAs (miRNAs) [13–16]. The induction of the senescent phenotype by genotoxic stress by 5-Br-2'-dU in B16F1 cells is little known. The role of ROCK2 in tumor cell cytoarchitecture and senescence, which miRNAs could modulate, may expand forward other molecules involved in cellular senescence, such as F-actin and VIM.

miRNAs are small non-coding RNAs (17–22 nt), post-transcriptional regulators of the gene expression. Changes in the expression of miRNA 138-5p and 455-3p affect proliferation, migration, and invasion through its molecular target, Rock2 mRNA [17,18]. However, the involvement of ROCK2, miRNAs 138-5p, and 455-3p in the cytoarchitecture and mobility of B16F1 melanoma cells exposed to 5-Br-2'-dU is limited. This study aimed to analyze ROCK2 and miRs 138-5p and 455-3p expressions in the highly metastatic B16F1 mouse melanoma cells and assess the effect on cell motility and invasion of 5-Br-2'-dU, a reported antitumoral agent [11,12,19].

We report that 5-Br-2'-dU induces greater B16 melanoma cell circularization, adhesion, and migration, associated with more significant F-actin polymerization, collapsed in the intermediate filaments vimentin and coinciding with a reciprocal decrease in Rock2 mRNA, miR-138-5p, and miR-455-3p expression and provide evidence that ROCK2 activity and miR-138-5p and miR-455-3p may promote tumoral mobility associated with the cell senescence phenotype induce for 5-Br-2'-dU in this model.

2. Materials and methods

2.1. Culture of the cell line B16F1 and viability assays

The mouse melanoma line B16F1 from the American Type Culture Collection® (CRL-6322 ™, Virginia, USA) was cultured in DMEM supplemented with 10% (v/v) fetal bovine serum (Gibco, Thermo Fisher Scientific, USA), penicillin (100 U/mL), and streptomycin (100 μg/mL) and incubated at 37 °C with 5% CO_2 and 98% humidity. We exposed an average of 1.5×10^5 B16F1 cells seeded in complete DMEM for 72 h to 5-Br-2'-dU [2.5 μg/mL] final concentration (Sigma-Aldrich). For all the assays for the inhibition of the activity of the mROCK2 protein, including cell viability, the inhibitor Y27632 ((R) - (+) - trans - 4 - (1-Aminoethyl) was added to cells exposed or not to 5-Br-2'-dU - N - (4-Pyridyl) cyclohexane carboxamide dihydrochloride)) (Calbiochem, La Jolla, California, USA) [10 μM] final concentration for 1 h.

2.2. Analysis of cell morphology

We incubated, on average, 2.0×10^3 B16F1 cells adhered to coverslips in the presence or absence of 5-Br-2'-dU. After 72 h, we took phase-contrast images in a 20x Nikon Eclipse Ti inverted light microscope (Kobe, Japan). The apparent cell area was quantified in the NIS-Elements-Nikon program by automatic cell counter for 100 cells per replicate. The values presented as an average ± SD with a significance level alpha = 0.05. For the diameter of cells in suspension, after exposure to 5-Br-2'-dU, the average cell size function was assessed with the Tali ™ Image-based Cytometer.

2.3. Cell complexity and size analysis by flow cytometry

We analyzed 1.0×10^4 cells on a BD FACSAria II™ flow cytometer (New Jersey, USA), and the degree of diffraction (FSC-A) and scattering (SSC-A) of light associated with size and granularity with the FlowJo™ program. Statistical significance was determined for n = 3, by multiple t-tests without correction, with an alpha = 0.05.

2.4. Wound healing test

B16F1 cells exposed to 5-Br-2'-dU, seeded in 24-well boxes up to 80% confluence and incubated for 1 h in the Y27632 inhibitor's presence, were wounded in the monolayer with a micropipette tip. Detached cells were removed with PBS and supplemented with incomplete DMEM (iDMEM). We calculated the percentage decrease in the area generated by the wound in photographs obtained in phase contrast of the Nikon Eclipse Ti microscope at 20x, at times 0 h, 3 h, 6 h, 12 h, 18 h, and 24 h with the NIS-Elements program. Statistical significance was determined for n = 3, by multiple t-tests without correction, with an alpha = 0.05.

2.5. Cell shedding dynamics

Cell circularity dynamics were carried out following previous reports [20,21], but adjusted for 1.0×10^3 B16F1 cells exposed or not to 5-Br-2'-dU and Y27632. In summary, cells washed with PBS were exposed to 50 μL per sheet of Trypsin-EDTA 0.25% (m/v), preheated to 37 °C, added, and captured in a Nikon Eclipse Ti microscope every 30 s, until the 600 s. We assessed the cell area variation from the microphotographs and Boltzmann normalization using the Prism-GraphPad program (https://www.graphpad.com/scientific-software/prism/). We counted the number of detached cells in each case determined by obtaining the non-adhered cells after the addition of trypsin-EDTA and quantification assessed on the Tali™ Image-based Cytometer.

2.6. Cell migration in the Boyden-type chamber

B16F1 cells previously exposed to 5-Br-2'-dU and Y27632 incubated for 12 h in DMEM. In the upper compartment of the Transwell™ chamber (Corning™), 100 μL of iDMEM seeded per well, containing, on average, 1.0×10^5 cells; we added 600 μL of complete DMEM in the lower compartment of the chamber as a chemo-attractant. After 24 h, we recovered from the upper chamber cells that did not penetrate the membrane with a cotton swab. We added 0.25% (m/v) Trypsin-EDTA to quantify the cells that crossed the membrane to both compartments and the collected cell suspension counted in Tali® image-based cytometer.

2.7. Immunocitofluorescence

Cells were fixed with 4% paraformaldehyde (m/v) in PBS and permeabilized with Triton™ X-100 0.3% (v/v) (Sigma-Aldrich). Anti-ROCK2 (sc-1851) (Santa Cruz Biotechnology. Inc, Dallas, USA) and exposed to anti-Vimentin (SAB4300676 Sigma-Aldrich) polyclonal antibodies as primary antibodies. In all cases, the final concentration of primary antibody was 0.4 μg/mL. As secondary antibodies, we used a Texas Red-labeled (sc-3923) or CFL-647 (sc-362292) at 0.15 μg/mL. For F-actin fiber staining, we incubated with 50 μg/mL of Faloidin conjugated with Fluorescein Isothiocyanate (FITC) (Sigma – Aldrich P5282) for 40 min at room temperature, and nuclei labeled with DAPI (4',6-diamidino-2-fenilindol) (Sigma-Aldrich). We obtained the images by using an inverted Nikon Eclipse Ti microscope. For quantifying the mean fluorescence intensities (MFI), we used the NIS-Elements program for n = 3 and an average of 100 cells per replicate and sample.

2.8. Western blot

We used 30 μg of protein per sample and fractionated in a 10% SDS-PAGE electrophoresis under denaturing conditions. The transferred proteins to a PVDF membrane (Millipore-Merck) in a Novex® Semi-Dry Blotter system (Thermo Fisher Scientific) following the manufacturer's recommendations were blocked with a solution of polyvinylpyrrolidone (PVP-40) (Sigma-Aldrich) at 1% (m/v) in PBS-Tween 20 (Sigma-Aldrich) [22] and incubated with the antibodies used in IF for mROCK2, mVIM or Lamin-B1 (sc-6216). As secondary anti-goat (PI-9500) or anti-rabbit (P1-1000) antibody, labeled with HRP (VECTOR, Burlingame-California, USA). The detection was carried out by the chemiluminescent method ECL-Western blotting system (Amersham, Boston, USA) following the manufacturer's recommendations and the

densitometric analysis assessed in Fiji - ImageJ (https://fiji.sc/), using as loading control detection of nuclear protein Lamin-B1.

2.9. Total RNA extraction and small RNA enrichment

Based on the method described [23,24], we extract total RNA following the organic extraction protocol with TRIzol-chloroform. For the enriched fractions of small RNAs ≤200 nt, we used the miRVana™ miRNA Isolation Kit (Ambion, Austin, USA) following the manufacturer's recommendations and quantified on a Nanodrop 2000 (Thermo Fisher Scientific).

2.10. RT-qPCR of mRNAs

For retro-transcription (RT), we used 2 ng of total RNA, oligo dT, and Superscript II reverse transcriptase (Invitrogen), following the manufacturer's recommendations: 50 min at 42 °C and then 15 min at 70 °C in a thermal cycler (BIO-RAD Hercules, California, USA). We used Real-time PCR (qPCR) in a BIO-RAD Chromo 4™ System thermocycler to analyze differential expression. In brief, each reaction contained 600 ng of cDNA as a template and primers corresponding to each gene evaluated (Supplementary Table 1) and the DyNAmo HS SYBR Green Kit (Thermo Fisher Scientific). The amplification conditions were one cycle of 95 °C 15 min, 36 cycles of 10 s at 96 °C, 30 s of annealing temperature according to each set of primers, and 30 s at 72 °C. We calculated the relative expression radius (rER) normalized by the expression of the housekeeping gene GAPDH [25].

2.11. RT-qPCR-stem-loop of miRNAs

The expression of miR-138-5p and miR-455-3p was evaluated by RT-qPCR stem-loop using miRVana™ microRNA Detection Kit (Thermo Fisher Scientific) under the manufacturer's recommendations. We used 65 ng of enriched RNA in Reverse transcriptions for 30 min at 16 °C, 30 min at 42 °C, and 5 min at 85 °C. For the qPCR, we used 2.5 μg of the cDNA, 3 min 95 °C, 40 cycles 15s 95 °C, 1 min 60 °C, 1 min at 72 °C, with a final extension of 10 min at 72 °C. We calculated the relative expression radius (rER) normalized by the expression of the housekeeping gene GAPDH [26].

2.12. Statistic analysis

The number of independent replications used in the statistical analyses was three, the values reported as a mean ± S.D. and the results were considered non-significant (ns) with $p > 0.05$, significant (*) with $p < 0.05$, very significant (**) with $p < 0.01$, highly significant (***) with $p < 0.001$ and very highly significant (****) with $p < 0.0001$. Using the software GraphPad Prism® (Graphpad Software Inc., La Jolla, CA, USA). We tested significant differences between each exposure and control using an unpaired Student t-test. In contrast, for multiple tests, the level of significance (we performed two-tailed multiple t-tests *) and differences were considered statistically significant for a $p < 0.05$ value using the Holm-Sidak method.

3. Results

3.1. Area and size of B16F1 cells after exposure to 5-Br-2'-dU

We performed an analysis of the apparent cell area to identify variations in the morphology of B16F1 cells exposed to 5-Br-2'-dU. Compared with the control (non-exposed cells), cells exposed to 5-Br-2'-dU showed a more extended and flattened morphology, fewer extensions, and an apparent decrease in the number of cells and pigmentation (Fig. 1A); previously reported changes in B16 [24–26] and other cellular models [27–29]. The apparent cell area increased by 2.2X ($3.2 \times 10^4 \pm 2$ EXP3 μm [2] and % CV 6.15) in exposed cells concerning the control ($1.4 \times 10^4 \pm 2$ EXP3 μm [2] and % CV 13.58) (Fig. 1B).

On the other hand, cells in suspension exposed to 5-Br-2'-dU increased their cell diameter by 1.27X, going from 12.0 ± 1.0 μm to 15.3 ± 0.57 μm (Fig. 1C). These results coincided with analyzing the population classification of suspended cells by light scattering (FSC-A). Light diffraction (SSC-A), in which the exposed cells showed a

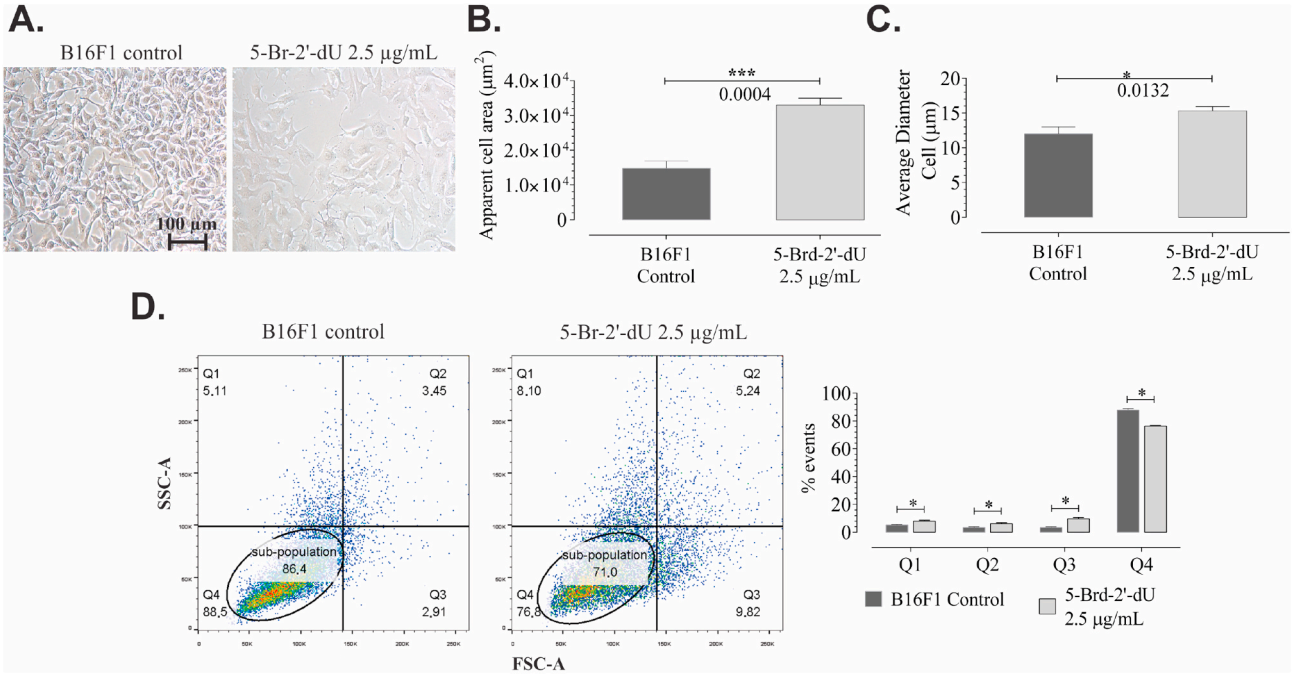

Fig. 1. Changes in the morphology and size of B16F1 cells after exposure for 72 h to 5-Br-2'-dU. A. Representative photographs of B16F1 cells exposed or not exposed to 5-Br-2'-dU 2.5 μg/mL. B. Measurement of Apparent cell area (μm [2]) determined from the contour of adhering cells. C. Average diameter (μm) of cells in suspension exposed or not to 5-Br-2'-dU. D. Representative diagrams obtained by a cytometry flow rate of the number of cells distributed by quartiles (Q) as a function of SSC-A and FSC-A and their percentages (Q1, Q2, Q3, and Q4) for three independent replicas with a total of 10,0000 events each.

displacement towards the Q1 quadrants (of 5.2 ± 0.3% to 7.9 ± 0.6%), Q2 (from 3.4 ± 0.4% to 6.0 ± 0.8%) and Q3 (from 3.4 ± 0.4% to 9 ± 1.0%), decreasing the percentage of cells in the control population (Q4) from 87, 83 ± 1.0% to 73.33 ± 0.5% (Fig. 1D). In the Q3 quadrant representing larger cells, a higher % CV (14.14) for control vs. exposed cells to 5-Br-2'-dU (10.7) suggested a more homogeneous pattern for the latter. Changes were associated with increased cellular organelles and the cytoskeleton's restructuring, which altered cell proliferation [30,31].

3.2. ROCK2 and VIM proteins expression involved in the cytoarchitecture of B16F1 cells exposed to 5-Br-2'-dU

Morphological changes induced by exposure to 5-Br-2'-dU coincided with mRNA expression changes [32,33] and β-actin cytoskeletal protein [34]. Therefore, we evaluated the eventual variation of ROCK2, VIM, and the polymerization of F-actin in this cellular model. When quantifying the mean fluorescence intensity (Fig. 2 A-B) of the ROCK2 protein, we found a 3X decrease in cells exposed to 5-Br-2'-dU compared to the control correlated with the Western blot results where the value was reduced 0.79X (Fig. 2C).

On the other hand, in control cells, the distribution of F-actin labeled with Faloidin-FITC showed a perinuclear localization, in contrast to the F-actin observed in 5-Br-2'-dU exposed cells, where the distribution of F-actin showed positivity throughout entire the all cytoplasm, more defined fibers, and an apparent more significant number of these were visualized (Fig. 2D). The addition of the ROCK2 inhibitor Y27632 in control cells showed no apparent changes in F-actin. In contrast, cells exposed to 5-Br-2'-dU shifted in shape and distribution, suggesting that 5-Br-2'-dU may induce downregulation of ROCK2 in B16F1. The high affinity of Y27632 for the ROCK family of kinases [35], actin fibers distributed throughout the cytoplasm with more stable adherent structures [36], and ROCK2 decrease in its expression, upon exposure to 5-Br-2'-dU, allow us to propose that ROCK2 are involved in the stability of polymerized F-actin.

We found a 2.02X increase in the expression level of VIM by Western Blot (Fig. 2F.) and distributed peri-nuclearly (Fig. 2E), a phenomenon also previously reported in cells with greater adhesion capacity. Possibly due to the binding of VIM to focal adhesion complexes [37]. These results are consistent with mechanisms that may facilitate efficient remodeling F-actin polymerization and ameboid-type mobility, as has already been described in melanoma cells [38]. ROCK2 and VIM proteins expression and the polymerization of F-actin suggested possible changes in the mobility of B16F1 cells after exposure to 5-Br-2'-dU.

3.3. Modifications in the cellular mobility of B16F1 exposed to 5-Br-2'-dU

We evaluated the phenomena of circularity, adhesion, and migration of B16F1 cells exposed to 5-Br-2'-dU and the Rock2 inhibitor Y27632. As visualized in Fig. 3A, the cells exposed to 5-Br-2'-dU presented a greater circularity concerning the control cells; and while, in exposed cells, the addition of Y27632 did not generate further modification, the cells exposed to 5-Br-2'-dU did show an apparent increase in their circularity.

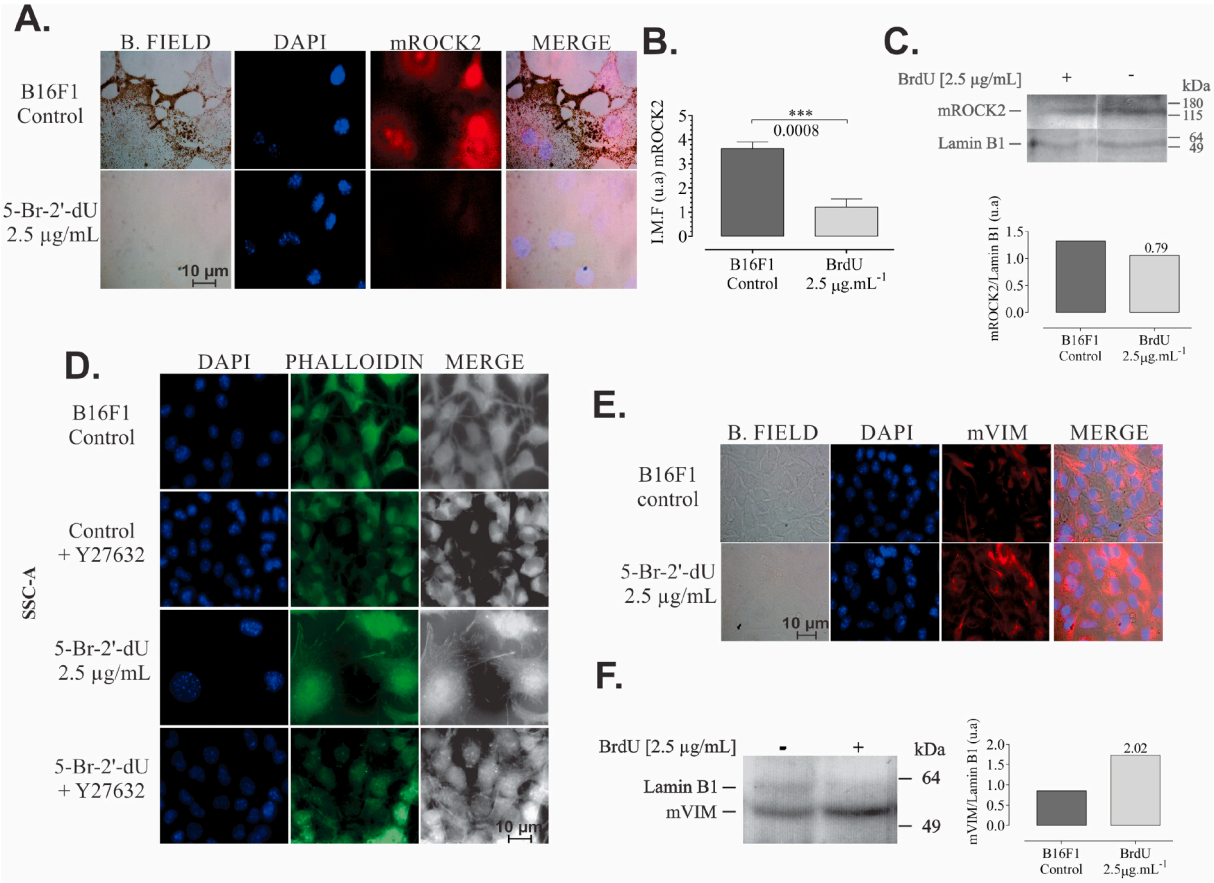

Fig. 2. Variation in mROCK2 and mVIM expression in B16F1 cells after exposure to 5-Br-2'-dU. Representative photographs of the location and distribution by immunofluorescence (IF) of the mROCK2 (A.) and mVIM (E.) proteins marked in red and quantified in arbitrary units of medium fluorescence intensity (MFI) of mROCK2 (B.). D. Microphotographs of F-actin marking with phalloidin-FITC (green) in B16F1 cells exposed to 5-Br-2'-dU and inhibitor **Y27632**. In A, D, and E against nuclear staining with DAPI (blue). Western blot and densitometry of mROCK2 in C. and mVIM in F; as load control, we used the nuclear protein Lamin-B1. (For interpretation of the references to colour in this figure legend, the reader is referred to the Web version of this article.)

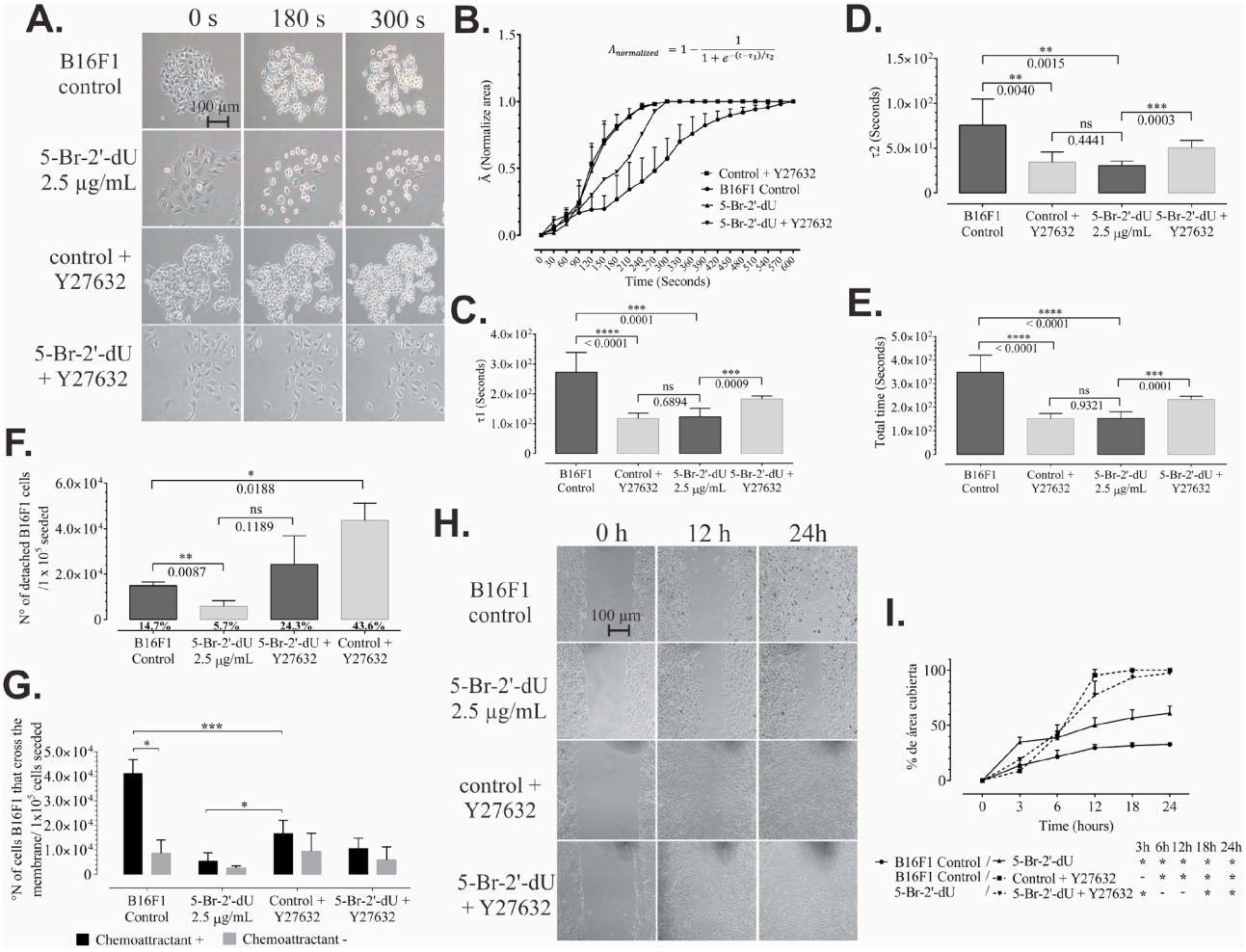

Fig. 3. Changes in circularity, adhesion, and migration of B16F1 cells after exposure to 5-Br-2'-dU. A. Representative images of time-lapse for circularity dynamics by trypsin-EDTA addition in B16F1 control cells exposed 5-Br-2'-dU and in the presence of inhibitor Y27632. B. Variation of the normalized area concerning time during the circularity test; C and D. The data fixed to an equation Boltzmann sigmoid to determine the time constants τ1 and τ2, respectively. E. We added τ1 and τ2 to calculate the total detachment time. F. Number of cells detached after addition of Trypsin-EDTA. G. Number of B16F1 cells passing through the membrane in a Boyden-type chamber after exposure to 5-Br-2'-dU and Y27632. H. Photographs from the wound healing assay for B16F1 cells exposed or not to 5-Br-2'-dU and inhibitor Y27632. I. Percentage of wound closure measured at 0 h, 3 h, 6 h, 12 h, 18 h, and 24 h. * Represents a statistical significance with a value $p < 0.05$.

These variations were quantified and represented as a normalized area as a function of time, which allowed the generation of sigmoid curves that suggested greater speed due to the shift to the left (Control + Y27632 and 5-Br-2'-dU 2.5 μg/mL) (Fig. 3. B). We confirmed these observations by quantifying the constants τ1, τ2, and τ1 + τ2 after Boltzmann normalization (Fig. 3C-E). The cells exposed to 5-Br-2'-dU presented shorter circularization times in all cases (τ1 = 123.04 ± 27.9; τ2 = 30.5 ± 4.9 and total time = 153.3 ± 28.3) compared to the circularization times for unexposed cells (τ1 = 272.3 ± 6.4; τ2 = 75.8 ± 28.8 and total time = 384.1 ± 72.2). The addition of Y27632 in the control cells showed a reduction in the circularization times (τ1 = 117.9 ± 17.2; τ2 = 34.3 ± 1.3, and total time = 152.2 ± 20.9), while in cells previously exposed to 5-Br-2'-dU, a slight increase in constants (τ1 = 182.7 ± 9.5; τ2 = 56.4 ± 8.2, and total time = 233.2 ± 13.2) (Fig. 3C-E). Decreased ROCK2 expression associated with increases in the circularization capacity of B16F1 cells due to the exposure to 5-Br-2'-dU identified possible modifications in cell mobility by exposure to 5-Br-2'-dU and the participation of ROCK2. Also, since the inhibitor's presence, the cells previously exposed to 5-Br-2'-dU do not completely circularize. It is possible that the low expression of ROCK2, added to its inhibition, activates other mechanisms that promote greater stability of the cell cytoskeleton.

When evaluating the differences in the percentage of cells shed from the substrate after the addition of Trypsin-EDTA, we found that the cells exposed to 5-Br-2'-dU maintained a lower percentage of shedding compared to the control cells (5.7% and 14.7%, respectively); This value increased by 43.6%, after the addition of Y27632, for control cells and not significantly for cells in the presence of 5-Br-2'-dU. These results suggest that shedding in exposed 5-Br-2'-dU cells would not be dependent on circularization but rather implies a decrease in the expression of ROCK2, redistribution adhesion, a phenomenon reported in different cell models [29,39–41]and associated with greater expression of integrins [42].

Regarding alterations in cell mobility, we evaluate Boyden chamber migration and wound healing tests for cells exposed to 5-Br-2'-dU and Y27632. Cells exposed to 5-Br-2'-dU with the ability to cross the membrane in the Boyden chamber decreased by 86.6% vs. cells without 5-Br-2'-dU (Fig. 3G). After the addition of Y27632, a reduction of 60%, while in cells exposed to 5-Br-2'-dU, there were no statistically significant changes. In the wound healing test, the exposure to 5-Br-2'-dU produced a more significant closure of the wound starting from 3 h vs. the control cells, and independent of the exposure to 5-Br-2'-dU, the addition of Y27632 increased the closing capacity, starting at 18 h (Fig. 3 H-I).

The evidence presented here suggests favoring different mobility

types to the differential expression of ROCK2 and VIM proteins. It was necessary to determine whether these expression levels coincided with changes in the expression of the corresponding mRNAs and the miR-138-5p and miR- 455-3p, which by predictors we described as potential regulators.

3.4. Variation in the expression of Rock2 and Vim mRNAs and miRNAs 138-5p and 455-3p in B16F1 cells exposed to 5-Br-2'-dU

To establish whether cells exposed to 5-Br-2'-dU showed changes in the expression of miR-138-5p and miR-455-3p and of the Rock2 mRNA, we used RT-qPCR assays. Compared with unexposed cells, the expression levels of Rock2 and miR-138-5p showed a decrease of 2.88X and 2.39X, respectively (Fig. 4A, D); meanwhile, miR-455-3p showed a 1.8X magnification (Fig. 4C). miR-138-5p and miR-455-3p had the potential to reduce the luciferase reporter gene expression through 3'UTR sequences of Rock2, suggesting Rock2 as a molecular target of these miRs [17,18,43]. Interestingly, humans and mice fully conserve these 3'UTR sequences' content (Fig. 4E), which suggests that in B16F1 cells, these two microRNAs would also have a regulatory potential on Rock2. These results would indicate that miR- 455-3p would have greater participation than miR-138-5p in the downward regulation of the Rock2 level, which would coincide with that observed in the protein product (Fig. 2A-C). As for Vim's mRNA, its expression level showed an increase of 3.64 X (Fig. 4B), coinciding with the increase in protein levels. Vim's increased expression may be a consequence of the under-expression found here for miR-138-5p (Fig. 4E), as Vim is a molecular target of miR-138-5p [44]. These results suggest that these and other miRNAs would regulate the variations in Vim and Rock 2 expression observed after exposure to 5-Br-2'-dU and that these variations would, in turn, have significant repercussions on mobility phenomena.

4. Discussion

Cancer cells in melanoma reorganize their cellular skeleton favoring migratory and invasive processes [45–47]. Exposure to the thymidine analog 5-Br-2'-dU generates a senescent phenotype in different cellular models [27,29,30], which implies the restructuring of the cellular cytoskeleton and variations in the expression of mRNAs and miRNAs involved in melanogenesis, cell cycle control, senescence in melanoma [15,16,33,34]. However, the association between structural variations and mobility of B16F1 cells is still unknown, as well as the involvement of ROCK2 and miRNAs mediate regulation would be related to mobility in other tumor models [47–51].

This article reports an increase in the apparent cell area, the diameter of cells in suspension, and cellular granularity (Fig. 1). These changes are consistent with other *in vitro* cell models, including fibroblasts [27], embryonic retinal pigment cells [28], lung cancer cells [29], and melanoma cells [30,52]. These changes could be associated with an increase in the cell complexity due to the number of organelles, for example, lysosomes, coinciding with the senescent phenotype [30,31]. Although the apparent cell area and the B16F1 cells' diameter exposed to 5-Br-2'-dU vs. control coincided in their upward trend, the rate of change between apparent area and diameter (1.74X). This variation suggests that the area's increase did not depend entirely on the increase in its cell size. One potential explanation could imply a greater capacity for an extension by these cells; in which case, there would be possible changes at the level of the reorganization of the cellular cytoskeleton and the expression of structural and regulator cytoskeletal proteins such as ROCK2 kinase, one of the central regulators of cytoskeletal restructuring [7,38].

In this regard, the B16F1 mouse melanoma cells exposed to 5-Br-2'-dU for 72 h show a decreased expression of ROCK2 (Fig. 2A-C), a decrease in the polymerization of actin stress fibers (Fig. 2D.), and a greater expression of the main component of the intermediate filaments VIM (Fig. 2E-F.), both processes regulated by ROCK2 [5,6], previously reported for cells with a senescent phenotype [53,54] and that are related to migration [7,38], metastasis [55,56], and amebic-type invasion in melanoma [57,58]. Although further work on variations in the phosphorylation of MLC or Cofilin, direct effectors of F-actin regulation, in the presence of Y27632, is necessary to confirm the involvement of ROCK2. The alterations in the cytoskeleton reported so far have not been quantified in other cells exposed to 5-Br-2'-dU and could suggest variations in the tumor mobility and mechanisms that regulate the expression of these genes, such as microRNAs.

Therefore, we evaluated the phenomena of cell adhesion, contractility, and migration in B16F1 cells exposed to 5-Br-2'-dU and ROCK2 inhibitor Y27632. There was an increase in the adhesion, circularization capacity, and wound closure capacity and a decrease in its Boyden chamber migration capacity (Fig. 3). Since the wound healing assay

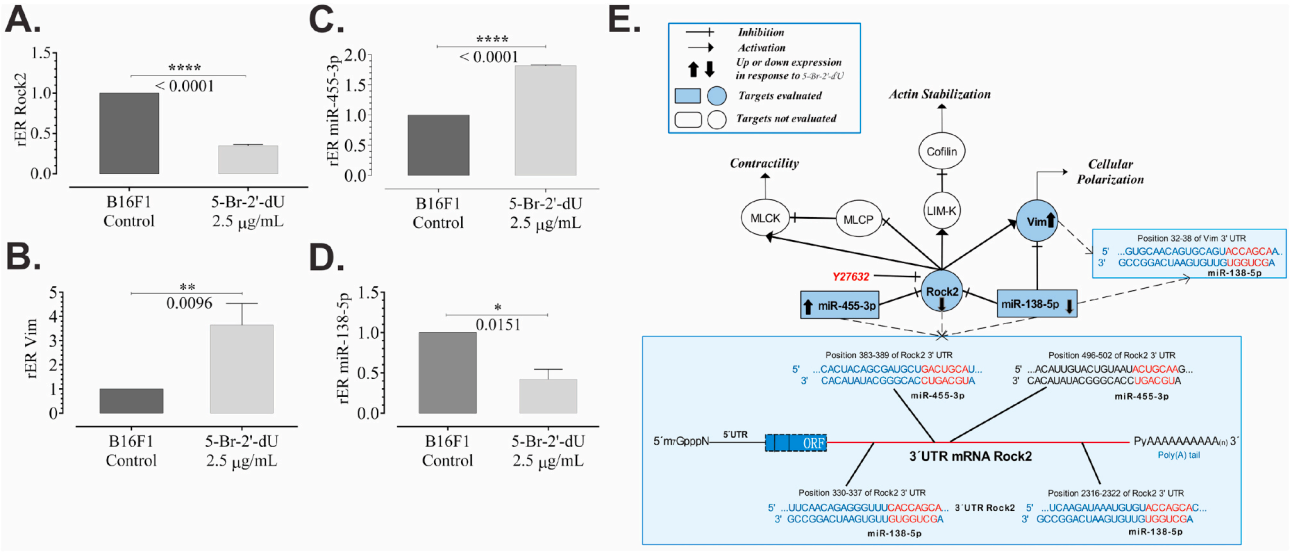

Fig. 4. Variation in Rock2, Vim, and miR-455-3p and miR-138-5p mRNA expression in B16F1 cells exposed to 5-Br-2'-dU. The radius of differential expression (rER) by RT-qPCR for Rock2 (A) and Vim (B) mRNAs normalized with the expression of the constitutive gene GAPDH. rER for miRNAs miR-455-3p (C) and miR-138-5p (D) determined by RT-qPCR stem-loop and normalized with the expression of snRNA U6. E. Scheme summarizing the possible regulation of miRNAs miR-455-3p and miR-138 5p on Rock2 and Vim expression and their association with mobility phenomena.

allows the evaluation of collective cell migration, favored by cell polarity [59] and also related to the perinuclear location of VIM [37] (Fig. 2E), these results are consistent with the reorganization of the cytoskeleton favoring adherence and this type of migration in B16F1 cells, possibly through the use of pseudopods and independent of ROCK2 regulation [60,61]. In contrast, control cells migrate 86.6% more in the Boyden chamber assay (Fig. 3G), consistent with a reorganization peri-nuclear F-actin (Fig. 2D), a critical role for ROCK2 associated with ameboid-like mobility [62,63].

The participation of F-actin regulators such as Cdc42/MRCK [53] and VIM intermediate filaments such as caspases [64], the use of Y27632, and its high affinity for ROCK kinases [35], suggests some involvement of this kinase in the variation of the motility phenomena evaluated here, however, knockout or silencing assays with RNA interference are still necessary.

The results observed in migration phenomena coincide with the decrease in Rock2 mRNA expression (Fig. 4A) and the differential expression of two miRs (138-5p downward and 455-3p upward) (Fig. 4. BC). This result is consistent with whose variations have recently linked to alterations in mobility in squamous cell cancer of the tongue and renal fibrosis [17,18] through their common molecular target Rock2. Small RNAseq sequencing results, recently obtained by our laboratory [16] confirmed the differential expression of these two microRNAs, but also of another set of microRNAs with high expression (129-5p, 30d-5p, 22 -3p, 335-5p, 193b-3p, and 144-3p) and to the low (211-5p, 128-3p and 23a-3p), that have Rock2 as a molecular target [44]. On the other hand, Vim's mRNA expression showed an increase of 3.64 X (Fig. 4B), a change that could be the consequence of direct regulation of miR-138-5p [44]. These results strengthen the hypothesis that the regulation mediated by microRNAs on Rock2 and Vim results from expression changes at the high and low levels of sets of microRNAs in which miR-455-3p and miR-138-5p participate, and that would be related to the morphological and proliferative changes observed in B16 melanoma cells from exposure to 5-Br-2'-dU.

The results reported so far are consistent with the coordinating role of ROCK2 in melanoma cell mobility [20,50,56] and contribute to the hypothesis of miRNA-mediated expression regulation as an anticancer therapy [3,65–67]. Additionally, experimental evidence on variations in tumor mobility related to the use of migration events [7,38], metastasis [55,56], and amebic-type invasion in melanoma [57,58], whose ability to induce senescence allows to propose as a chemotherapeutic adjuvant that enhances anti-tumor activity [29]. We believe that future trials should focus on experimentally confirming the functional association of miRNAs 138-5p and 455-3p with Rock2, as well as evaluating the collective participation of other molecular targets and transcription factors eventually involved in these cytoskeletal reorganization pathways, such as RhoC, another molecular target of miR-138-5p [17,67].

Sample CRediT author statement

Esther Natalia Muñoz: Methodology, Validation, Investigation, Visualization, Writing - Original Draft. **Hernán Mauricio Rivera:** Methodology, Validation, Formal analysis, Investigation, Visualization, Writing - Original Draft. **Luis Alberto Gómez:** Conceptualization, Methodology, Writing - Review & Editing, Supervision.

Funding

The Instituto Nacional de Salud de Colombia funded this research. Project-grant No. CETIN-01-2016. MRS had a fellowship from COLCIENCIAS.

Declaration of competing interest

The authors declare that they have no known competing financial interests or personal relationships that could have appeared to influence the work reported in this paper.

Acknowledgments

The authors thank the Instituto Nacional de Colombia (INS), COLCIENCIAS, and the Universidad Nacional de Colombia (UNAL).

Appendix A. Supplementary data

Supplementary data to this article can be found online at https://doi.org/10.1016/j.bbrep.2021.101027.

References

[1] G.P. Guy, C.C. Thomas, T. Thompson, M. Watson, G.M. Massetti, L.C. Richardson, Vital signs: melanoma incidence and mortality trends and projections — United States, 1982–2030, MMWR Morb. Mortal. Wkly. Rep. 64 (21) (2015) 591–596. http://www.ncbi.nlm.nih.gov/pmc/articles/PMC4584771/.

[2] A. Esteva, B. Kuprel, R.A. Novoa, et al., Dermatologist-level classification of skin cancer with deep neural networks, Nature 542 (2017) 115, https://doi.org/10.1038/nature21056.

[3] M. Nakajima, K. Hayashi, Y. Egi, et al., Effect of Wf-536, a novel ROCK inhibitor, against metastasis of B16 melanoma, Canc. Chemother. Pharmacol. 52 (4) (2003) 319–324, https://doi.org/10.1007/s00280-003-0641-9.

[4] A. Routhier, M. Astuccio, D. Lahey, et al., Pharmacological inhibition of Rho-kinase signaling with Y-27632 blocks melanoma tumor growth, Oncol. Rep. 23 (3) (2010) 861–867, https://doi.org/10.3892/or_00000708.

[5] W.C. Sin, X.Q. Chen, T. Leung, L. Lim, RhoA-binding kinase alpha translocation is facilitated by the collapse of the vimentin intermediate filament network, Mol. Cell Biol. 18 (11) (1998) 6325–6339, https://doi.org/10.1128/mcb.18.11.6325.

[6] M. Amano, M. Ito, K. Kimura, et al., Phosphorylation and activation of myosin by rho-associated kinase (Rho-kinase), J. Biol. Chem. 271 (34) (1996) 20246–20249, https://doi.org/10.1074/jbc.271.34.20246.

[7] G. Totsukawa, Y. Yamakita, S. Yamashiro, D.J. Hartshorne, Y. Sasaki, F. Matsumura, Distinct roles of ROCK (Rho-kinase) and MLCK in spatial regulation of MLC phosphorylation for assembly of stress fibers and focal adhesions in 3T3 fibroblasts, J. Cell Biol. 150 (4) (2000) 797–806. https://www.ncbi.nlm.nih.gov/pubmed/10953004.

[8] C. López-Otín, M.A. Blasco, L. Partridge, M. Serrano, G. Kroemer, The hallmarks of aging, Cell 153 (6) (2013) 1194–1217, https://doi.org/10.1016/j.cell.2013.05.039.

[9] O. Moujaber, F. Fishbein, N. Omran, et al., Cellular senescence is associated with reorganization of the microtubule cytoskeleton, Cell. Mol. Life Sci. 76 (6) (2019) 1169–1183, https://doi.org/10.1007/s00018-018-2999-1.

[10] M. Kaczorowski, P. Biecek, P. Donizy, M. Pieniążek, R. Matkowski, A. Hałoń, ROCK1 and ROCK2 are down-regulated in aggressive and advanced skin melanomas – a clinicopathological perspective, Anticancer Res. 40 (4) (2020) 1931–1942, https://doi.org/10.21873/anticanres.14148.

[11] B. Djordjevic, W. Szybalski, Genetics of human cell lines. III. Incorporation of 5-bromo- and 5-iododeoxyuridine into the deoxyribonucleic acid of human cells and its effect on radiation sensitivity, J. Exp. Med. 112 (3) (1960) 509–531, https://doi.org/10.1084/jem.112.3.509.

[12] M.D. Prados, W. Seiferheld, H.M. Sandler, et al., Phase III randomized study of radiotherapy plus procarbazine, lomustine, and vincristine with or without BUdR for treatment of anaplastic astrocytoma: final report of RTOG 9404, Int. J. Radiat. Oncol. Biol. Phys. 58 (4) (2004) 1147–1152, https://doi.org/10.1016/j.ijrobp.2003.08.024.

[13] L. Gómez, M. Rieber, M. Rieber, PCR-mediated differential display and cloning of a melanocyte gene decreased in malignant melanoma and up-regulated with sensitization to DNA damage, DNA Cell Biol. 15 (5) (1996) 423–427, https://doi.org/10.1089/dna.1996.15.423.

[14] L.M. Escobar, Expresión diferencial del gen Rock alfa e inhibición del crecimiento de células de melanoma humano y murino inducido por la Genisteina y la L-Tirosina in vitro, 2001. Published online.

[15] Ó.R. Flórez Vargas, L.A. Gomez, Expresión diferencial de dos microRNAs asociados con el silenciamiento de la ciclina D1 en células de melanoma B16 en senescencia inducida por la 5-bromo-2-desoxiuridina. Rev la Asoc Colomb Ciencias Biológicas, Published online, http://ezproxy.unal.edu.co/login?url=http://search.ebscohost.com/login.aspx?direct=true&db=cat02704a&AN=unc.000385548&lang=es&site=eds-live, 2008.

[16] H.M. Rivera, E.N. Muñoz, D. Osuna, M. Florez, M. Carvajal, L.A. Gómez, Reciprocal changes in miRNA expression with pigmentation and decreased proliferation induced in mouse B16F1 melanoma cells by l-tyrosine and 5-bromo-2′-deoxyuridine, Int. J. Mol. Sci. 22 (4) (2021), https://doi.org/10.3390/ijms22041591.

[17] L. Jiang, X. Liu, A. Kolokythas, et al., Downregulation of the Rho GTPase signaling pathway is involved in the microRNA-138-mediated inhibition of cell migration and invasion in tongue squamous cell carcinoma, Int J cancer 127 (3) (2010) 505–512, https://doi.org/10.1002/ijc.25320.

[18] J. Wu, J. Liu, Y. Ding, et al., MiR-455-3p suppresses renal fibrosis through repression of ROCK2 expression in diabetic nephropathy, Biochem. Biophys. Res. Commun. 503 (2) (2018) 977–983, https://doi.org/10.1016/J.BBRC.2018.06.105.

[19] L.N. Peñaloza Niño, Expresión del gen PRL-1, en células de melanoma murino B-16, inducidas a supresión del crecimiento con el sensibilizador a la radiación ultravioleta: bromodeoxiuridina TT - expression of the PRL-1 gene in B-16 murine melanoma cells induce to growth suppr, Published online, https://pesquisa.bvsalud.org/portal/resource/es/lil-278179, 2000.

[20] S. Srinivasan, V. Ashok, S. Mohanty, et al., Blockade of Rho-associated protein kinase (ROCK) inhibits the contractility and invasion potential of cancer stem like cells, Oncotarget 8 (13) (2017). Published online, https://www.oncotarget.com/article/15248/.

[21] S. Sen, S. Kumar, Cell-matrix de-adhesion dynamics reflect contractile mechanics, Cell. Mol. Bioeng. 2 (2) (2009) 218–230, https://doi.org/10.1007/s12195-009-0057-7.

[22] J.W. Haycock, Polyvinylpyrrolidone as a blocking agent in immunochemical studies, Anal. Biochem. 208 (2) (1993) 397–399, https://doi.org/10.1006/abio.1993.1068.

[23] P. Chomczynski, N. Sacchi, Single-step method of RNA isolation by acid guanidinium thiocyanate-phenol-chloroform extraction, Anal. Biochem. 162 (1) (1987) 156–159, https://doi.org/10.1016/0003-2697(87)90021-2.

[24] B. Ryu, D.S. Kim, A.M. Deluca, R.M. Alani, Comprehensive expression profiling of tumor cell lines identifies molecular signatures of melanoma progression, PLoS One 2 (7) (2007) e594, https://doi.org/10.1371/journal.pone.0000594.

[25] J.R. Wrathall, C. Oliver, S. Silagi, E. Essner, Suppression of pigmentation in mouse melanoma cells by 5-bromodeoxyuridine: effects on tyrosinase activity and melanosome formation, J. Cell Biol. 57 (2) (1973) 406–423, https://doi.org/10.1083/jcb.57.2.406.

[26] J.H. Schefe, K.E. Lehmann, I.R. Buschmann, T. Unger, H. Funke-Kaiser, Quantitative real-time RT-PCR data analysis: current concepts and the novel "gene expression's CT difference" formula, J. Mol. Med. (Berl.) 84 (11) (2006) 901–910, https://doi.org/10.1007/s00109-006-0097-6.

[27] B.T. Hill, A. Tsuboi, R. Baserga, Effect of 5-bromodeoxyuridine on chromatin transcription in confluent fibroblasts, Proc. Natl. Acad. Sci. U. S. A. 71 (2) (1974) 455–459, https://doi.org/10.1073/pnas.71.2.455.

[28] R.I. Garcia, I. Werner, G. Szabo, Effect of 5-bromo-2′-deoxyuridine on growth and differentiation of cultured embryonic retinal pigment cells, In Vitro 15 (10) (1979) 779–788, https://doi.org/10.1007/BF02618304.

[29] J.C. Masterson, S. O'Dea, 5-Bromo-2-deoxyuridine activates DNA damage signalling responses and induces a senescence-like phenotype in p16-null lung cancer cells, Anti Canc. Drugs 18 (9) (2007) 1053–1068, https://doi.org/10.1097/CAD.0b013e32825209f6.

[30] G.J. Giotta, K.W. Brunson, R. Lotan, The effects of 5-bromodeoxyuridine on cyclic AMP levels and cytoskeletal organization in malignant melanoma cells, Cell Biol. Int. Rep. 4 (1) (1980) 105–116, https://doi.org/10.1016/0309-1651(80)90015-6.

[31] W.L. Epstein, K. Fukuyama, T.E. Drake, Ultrastructural Effects of Thymidine Analogs on Melanosomes and Virus Activation in Cloned Hamster Melanoma Cells in Culture, vol. 46, 1973. https://www.ncbi.nlm.nih.gov/pmc/articles/PMC2592023/pdf/yjbm00160-0147.pdf. (Accessed 5 June 2019).

[32] R.H. Stellwagen, G.M. Tomkins, Differential effect of 5-bromodeoxyuridine on the concentrations of specific enzymes in hepatoma cells in culture, Proc. Natl. Acad. Sci. U. S. A. 68 (6) (1971) 1147–1150. http://www.jstor.org/stable/60292.

[33] P.M. Price, The effect of 5-bromodeoxyuridine on messenger RNA production in cultured cells, Biochim. Biophys. Acta Nucleic Acids Protein Synth. 447 (3) (1976) 304–311, https://doi.org/10.1016/0005-2787(76)90053-8.

[34] L. Gómez, M. Rieber, M. Rieber, Decrease in actin gene expression in melanoma cells compared to melanocytes is partly counteracted by BrdU-induced cell adhesion and antagonized by L-tyrosine induction of terminal differentiation, Biochem. Biophys. Res. Commun. 216 (1) (1995).

[35] S. Narumiya, T. Ishizaki, M. Ufhata, Use and properties of ROCK-specific inhibitor Y-27632, in: W.E. Balch, C.J. Der, A.B.T.-M. Hall (Eds.), Regulators and Effectors of Small GTPases - Part D: Rho Family, vol. 325, Academic Press, 2000, pp. 273–284, https://doi.org/10.1016/S0076-6879(00)25449-9.

[36] A.J. Ridley, A. Hall, The small GTP-binding protein rho regulates the assembly of focal adhesions and actin stress fibers in response to growth factors, Cell 70 (3) (1992) 389–399, https://doi.org/10.1016/0092-8674(92)90163-7.

[37] E. Terriac, G. Coceano, Z. Mavajian, et al., Vimentin levels and serine 71 phosphorylation in the control of cell-matrix adhesions, migration speed, and shape of transformed human fibroblasts, Cells 6 (1) (2017), https://doi.org/10.3390/cells6010002.

[38] V. Sanz-Moreno, C. Gaggioli, M. Yeo, et al., ROCK and JAK1 signaling cooperate to control actomyosin contractility in tumor cells and stroma, Canc. Cell 20 (2) (2011) 229–245, https://doi.org/10.1016/j.ccr.2011.06.018.

[39] M. Rieber, M.S. Rieber, C. Urbina, R. Lira, Differential response of adherent and unanchored melanoma cells to bromodeoxyuridine evidenced by specific lectin-binding protein changes, Int J cancer 43 (5) (1989) 841–844, https://doi.org/10.1002/ijc.2910430517.

[40] S. Githens, R. Pictet, P. Phelps, W.J. Rutter, 5-bromodeoxyuridine may alter the differentiative program of the embryonic pancreas, J. Cell Biol. 71 (2) (1976) 341–356, https://doi.org/10.1083/jcb.71.2.341.

[41] J. Abbott, H. Holtzer, The loss of phenotypic traits by differentiated cells, V. The effect of 5-bromodeoxyuridine on cloned chondrocytes, Proc. Natl. Acad. Sci. U. S. A. 59 (4) (1968) 1144–1151, https://doi.org/10.1073/pnas.59.4.1144.

[42] P. Meleady, M. Clynes, Bromodeoxyuridine induces integrin expression at transcriptional (α2 subunit) and post-transcriptional (β1 subunit) levels, and alters the adhesive properties of two human lung tumour cell lines, Cell Commun. Adhes. 8 (2001) 45–59.

[43] Z. Zhu, J. Tang, J. Wang, G. Duan, L. Zhou, X. Zhou, MiR-138 acts as a tumor suppressor by targeting EZH2 and enhances cisplatin-induced apoptosis in osteosarcoma cells, in: A. Ahmad (Ed.), PLoS One 11 (3) (2016), e0150026, https://doi.org/10.1371/journal.pone.0150026.

[44] J. Zhang, D. Liu, Z. Feng, et al., MicroRNA-138 modulates metastasis and EMT in breast cancer cells by targeting vimentin, Biomed. Pharmacother. 77 (2016) 135–141, https://doi.org/10.1016/j.biopha.2015.12.018.

[45] H. Byers, T. Etoh, J. Doherty, A.J. Sober, M. Mihm Jr., Cell migration and actin organization in cultured human primary, recurrent cutaneous and metastatic melanoma. Time-lapse and image analysis, Am. J. Pathol. 139 (2) (1991) 423–435. https://pubmed.ncbi.nlm.nih.gov/1867326.

[46] J. Bonaventure, M.J. Domingues, L. Larue, Cellular and molecular mechanisms controlling the migration of melanocytes and melanoma cells, Pigment Cell Melanoma Res 26 (3) (2013) 316–325, https://doi.org/10.1111/pcmr.12080.

[47] J.L. Orgaz, E. Crosas-Molist, A. Sadok, et al., Myosin II reactivation and cytoskeletal remodeling as a hallmark and a vulnerability in melanoma therapy resistance, Canc. Cell 37 (1) (2020), https://doi.org/10.1016/j.ccell.2019.12.003, 85-103.e9.

[48] M. El-Sibai, O. Pertz, H. Pang, et al., RhoA/ROCK-mediated switching between Cdc42- and Rac1-dependent protrusion in MTLn3 carcinoma cells, Exp. Cell Res. 314 (7) (2008) 1540–1552, https://doi.org/10.1016/j.yexcr.2008.01.016.

[49] D. Rösel, J. Brábek, O. Tolde, et al., Up-regulation of rho/ROCK signaling in sarcoma cells drives invasion and increased generation of protrusive forces, Mol. Canc. Res. 6 (9) (2008) 1410–1420. http://mcr.aacrjournals.org/content/6/9/1410.abstract.

[50] S. Kümper, F.K. Mardakheh, A. McCarthy, et al., Rho-associated kinase (ROCK) function is essential for cell cycle progression, senescence and tumorigenesis, Elife 5 (2016), https://doi.org/10.7554/eLife.12203 e12994-e12994.

[51] Y. Peng, Z. Chen, Y. Chen, et al., ROCK isoforms differentially modulate cancer cell motility by mechanosensing the substrate stiffness, Acta Biomater. 88 (2019) 86–101, https://doi.org/10.1016/j.actbio.2019.02.015.

[52] Selma Silagi, Modification of malignancy by 5-bromodeoxyuridine: studies of reversibility and immunological effects, Soc Vitr Biol 7 (1971). (Accessed 20 May 2019).

[53] I. Tan, C.H. Ng, L. Lim, T. Leung, Phosphorylation of a novel myosin binding subunit of protein phosphatase 1 reveals a conserved mechanism in the regulation of actin cytoskeleton*, J. Biol. Chem. 276 (24) (2001) 21209–21216, https://doi.org/10.1074/jbc.M102615200.

[54] K. Nishio, A. Inoue, Senescence-associated alterations of cytoskeleton: extraordinary production of vimentin that anchors cytoplasmic p53 in senescent human fibroblasts, Histochem. Cell Biol. 123 (3) (2005) 263–273, https://doi.org/10.1007/s00418-005-0766-5.

[55] S. Liu, R.H. Goldstein, E.M. Scepansky, M. Rosenblatt, Inhibition of rho-associated kinase signaling prevents breast cancer metastasis to human bone, Canc. Res. 69 (22) (2009) 8742–8751, https://doi.org/10.1158/0008-5472.CAN-09-1541.

[56] D. Vigil, T.Y. Kim, A. Plachco, et al., ROCK1 and ROCK2 are required for non-small cell lung cancer anchorage-independent growth and invasion, Canc. Res. 72 (20) (2012) 5338–5347, https://doi.org/10.1158/0008-5472.CAN-11-2373.

[57] J.L. Orgaz, P. Pandya, R. Dalmeida, et al., Diverse matrix metalloproteinase functions regulate cancer amoeboid migration, Nat. Commun. 5 (1) (2014) 4255, https://doi.org/10.1038/ncomms5255.

[58] G. Cantelli, J.L. Orgaz, I. Rodriguez-Hernandez, et al., TGF-β-Induced transcription sustains amoeboid melanoma migration and dissemination, Curr. Biol. 25 (22) (2015) 2899–2914, https://doi.org/10.1016/j.cub.2015.09.054.

[59] J.E.N. Jonkman, J.A. Cathcart, F. Xu, et al., An introduction to the wound healing assay using live-cell microscopy, Cell Adhes. Migrat. 8 (5) (2014) 440–451, https://doi.org/10.4161/cam.36224.

[60] C.D. Nobes, A. Hall, Rho, Rac, and Cdc42 GTPases regulate the assembly of multimolecular focal complexes associated with actin stress fibers, lamellipodia, and filopodia, Cell 81 (1) (1995) 53–62, https://doi.org/10.1016/0092-8674(95)90370-4.

[61] J.V. Small, K. Rottner, I. Kaverina, K.I. Anderson, Assembling an actin cytoskeleton for cell attachment and movement, Biochim. Biophys. Acta Mol. Cell Res. 1404 (3) (1998) 271–281, https://doi.org/10.1016/S0167-4889(98)00080-9.

[62] E. Sahai, C.J. Marshall, Differing modes of tumour cell invasion have distinct requirements for Rho/ROCK signalling and extracellular proteolysis, Nat. Cell Biol. 5 (8) (2003) 711–719, https://doi.org/10.1038/ncb1019.

[63] J.B. Wyckoff, S.E. Pinner, S. Gschmeissner, J.S. Condeelis, E. Sahai, ROCK- and myosin-dependent matrix deformation enables protease-independent tumor-cell invasion in vivo, Curr. Biol. 16 (15) (2006) 1515–1523, https://doi.org/10.1016/j.cub.2006.05.065.

[64] Y. Byun, F. Chen, R. Chang, M. Trivedi, K.J. Green, V.L. Cryns, Caspase cleavage of vimentin disrupts intermediate filaments and promotes apoptosis, Cell Death Differ. 8 (5) (2001) 443–450, https://doi.org/10.1038/sj.cdd.4400840.

[65] F. Peng, J. Jiang, Y. Yu, et al., Direct targeting of SUZ12/ROCK2 by miR-200b/c inhibits cholangiocarcinoma tumourigenesis and metastasis, Br. J. Canc. 109 (12) (2013) 3092–3104, https://doi.org/10.1038/bjc.2013.655.

[66] X. Li, J. He, M. Shao, et al., Downregulation of miR-218-5p promotes invasion of oral squamous cell carcinoma cells via activation of CD44-ROCK signaling, Biomed. Pharmacother. 106 (2018) 646–654, https://doi.org/10.1016/j.biopha.2018.06.151.

[67] H. Zheng, D. Ramnaraign, B.A. Anderson, E. Tycksen, R. Nunley, A. McAlinden, MicroRNA-138 inhibits osteogenic differentiation and mineralization of human dedifferentiated chondrocytes by regulating RhoC and the actin cytoskeleton, JBMR plus 3 (2) (2018), https://doi.org/10.1002/jbm4.10071 e10071-e10071.